Biochimica et Biophysica Acta 1837 (2014) 761–772

Contents lists available at ScienceDirect

Biochimica et Biophysica Acta

journal homepage: www.elsevier.com/locate/bbabio

Interactions involved in grasping and locking of the inhibitory peptide IF1 by mitochondrial ATP synthase

Qian Wu [a,1], Tiona Andrianaivomananjaona [a,1], Emmanuel Tetaud [b], Vincent Corvest [a,2], Francis Haraux [a,*]

[a] UMR 8221, CNRS-CEA-Université Paris-Sud, iBiTec-S, CEA Saclay, 91191 Gif-sur-Yvette, France
[b] Institut de Biochimie et Génétique Cellulaires, UMR 5095 CNRS, Université Victor Segalen, 1, rue Camille Saint Saëns, 33077 Bordeaux, France

ARTICLE INFO

Article history:
Received 30 August 2013
Received in revised form 24 January 2014
Accepted 29 January 2014
Available online 7 February 2014

Keywords:
ATP synthase
IF1 inhibitory peptide
Mitochondrion
Kinetics
Protein–protein interaction
Regulation

ABSTRACT

When mitochondria become deenergized, futile ATP hydrolysis is prevented by reversible binding of an endogenous inhibitory peptide called IF1 to ATP synthase. Between initial IF1 binding and IF1 locking the enzyme experiences large conformational changes. While structural studies give access to analysis of the dead-end inhibited state, transient states have thus far not been described. Here, we studied both initial and final states by reporting, for the first time, the consequences of mutations of *Saccharomyces cerevisiae* ATP synthase on its inhibition by IF1. Kinetic studies allowed the identification of amino acids or motifs of the enzyme that are involved in recognition and/or locking of IF1 α-helical midpart. This led to an outline of IF1 binding process. In the recognition step, protruding parts of α and especially β subunits grasp IF1, most likely by a few residues of its α-helical midpart. Locking IF1 within the αβ interface involves additional residues of both subunits. Interactions of the α and β subunits with the foot of the γ subunit might contribute to locking and stabilizing of the dead-end state.

1. Introduction

ATP synthase, also called F_0F_1-ATPase, plays a key role in cell energetics. This enzymatic complex is anchored to bacterial, chloroplastic and mitochondrial energy-transducing membranes. It consists of a membranous sector (F_0) and an extrinsic subcomplex (F_1). It synthesizes ATP, the main biological energy vector, at the expense of a transmembrane electrochemical proton gradient also called protonmotive force (*pmf*) [1]. ATP synthase is a molecular motor driven by protons [2]. A downhill proton flow through the F_0 sector rotates a cylindrical homo-oligomer containing 8 or 10 transmembrane c subunits [3,4] in the case of mitochondria. This cylinder is bound to the central shaft (γδε subunits) of the extrinsic part of the complex. The rotation is thus transmitted to the γ subunit, which sequentially distorts the three catalytic sites located at the interfaces of the peripheral α and β subunits arranged in a $(\alpha\beta)_3$ crown-like structure. These conformational changes induce binding of ADP and inorganic phosphate (P_i), their condensation into ATP and the release of ATP, according to the classical "binding-change" mechanism [5]. Viewed from the membrane, the central shaft rotates clockwise during ATP synthesis and in the opposite direction during ATP hydrolysis [2,6]. The direction of the reaction depends on the energetic balance between the *pmf* and the Gibbs free energy of the reaction, determined by ADP, P_i and ATP concentrations.

The activity of ATP synthase is regulated. Collapse of the *pmf*, which should theoretically trigger ATP hydrolysis, actually leads to enzyme inhibition. In mitochondria, this process involves a regulatory peptide called IF1 [7]. IF1 is a soluble peptide, 84 residue-long in *Bos taurus* and 63 residue-long in *Saccharomyces cerevisiae* [8]. Its structure is α-helical, except for its N-terminal extremity [9–11]. X-ray crystallographic structures of bovine and yeast F_1-ATPases, with or without bound IF1, have been published and revealed that the three catalytic (αβ) interfaces are in different conformations. These interfaces are named (αβ)TP, (αβ)DP and (αβ)E. This nomenclature was given according to the catalytic nucleotide occupancy (ATP analogue, ADP or empty) in the first published structure [12], and more generally to the rotor orientation which determines interface conformations even in the absence of nucleotides [13]. In crystallized bovine and yeast F_1-ATPase in complex with IF1, the inhibitory peptide interacts with α, β and γ subunits. The middle part of IF1 is inserted in the (αβ)DP catalytic interface. The N-terminal part mainly interacts with the central axis of the γ subunit and also with the α_E subunit. The C-terminal part is truncated in the bovine crystal and not visible in the yeast crystal [10,11].

When the inner membrane is deenergized, IF1 binds to the catalytic part of ATP synthase and blocks ATP hydrolysis. As soon as the *pmf* is

Abbreviations: F_0F_1-ATPase, ATP synthase complex (EC 3.6.3.14); F_1-ATPase, isolated extrinsic part of ATP synthase; IF1, endogenous inhibitory peptide of mitochondrial ATP synthase; yIF1, IF1 from yeast; SMP, submitochondrial particle; *pmf*, protonmotive force; Tris, tris(hydroxymethyl)aminomethane; MES, 2-(N-morpholino)ethanesulfonic acid; FCCP, carbonyl cyanide-p-trifluoromethoxyphenylhydrazone; Ni-NTA, nickel-nitrilotriacetic acid; PGK, phosphoglycerate kinase; KanMX4, kanamycin-resistance gene; G418, geneticine

* Corresponding author. Tel.: +33 1 69 08 98 91; fax: +33 1 69 08 87 17.
E-mail addresses: qian.wu@cea.fr (Q. Wu), tiona.andrianaivomananjaona@cea.fr (T. Andrianaivomananjaona), tetaud@ibgc.cnrs.fr (E. Tetaud), vcorvest@calixar.com (V. Corvest), francis.haraux@cea.fr (F. Haraux).
[1] Contributed equally to this work.
[2] Present address: Calixar, 7 Passage du Vercors, 69007 Lyon, France.

0005-2728/$ – see front matter © 2014 Elsevier B.V. All rights reserved.
http://dx.doi.org/10.1016/j.bbabio.2014.01.023

restored, the affinity of IF1 for ATP synthase dramatically decreases. This leads to its release and therefore allows the enzyme catalyzing ATP synthesis [14–21]. The reason for this *pmf*-dependent binding/release is not yet understood, and its elucidation requires analysis of IF1 binding dynamics. IF1 tight binding in the absence of *pmf* requires catalytic turnover, because it only occurs in the presence of ATP, and not in the presence of its non-hydrolysable analogue AMP-P-NP [22]. Previous studies with the isolated F_1-ATPase subcomplex have distinguished a first step, in which IF1 loosely binds to a catalytic site in an adequate conformation, and a second step, turnover-dependent, in which it is trapped within the complex [23,24]. Kinetic experiments using IF1 with the N-terminal extremity deleted [25,26] or attached to a globular protein suggested that this part of IF1 is not involved in the recognition step but contributes to the stability of the inhibited complex [25].

In this work, we identified amino acids or motifs of F_1-ATPase involved in the different steps of IF1 binding process. First, we mutated residues of *S. cerevisiae* ATP synthase selected on the basis of structures of the IF1-inhibited F_1-ATPase complex. Then, using submitochondrial particles prepared from wild type and mutated cells, we studied the kinetics of inhibition of ATP hydrolysis by IF1. For the first time, the effect of mutations of α, β and γ subunits on IF1 binding parameters (k_{on}, K_d and k_{off}) was observed. These data reveal how the set of interactions between IF1 and F_1-ATPase subunits varies between IF1 grasping and formation of the dead-end state. Moreover, they bring a new insight on the inhibition process by suggesting that α–γ and β–γ interactions contribute to the stabilization of the inhibited complex.

2. Materials and methods

2.1. Mutagenesis of α subunit and β subunit

α subunit and β subunit mutagenesis was achieved by transforming *Δatp1* and/or *Δatp2 S. cerevisiae* cells with plasmids containing WT or mutated *ATP1* and/or *ATP2* genes, respectively. The plasmid containing *ATP1* gene was obtained by modifying the plasmid pFL61 [27] as following. First, the 2-micron replication origin was replaced by the ARS/CEN replication origin. Then, the coding DNA sequence of *ATP1* gene was inserted into this plasmid under the control of PGK promoter and terminator, leading to the plasmid pVC2-ATP1. The plasmid with *ATP2* gene was pRS313/ATP2-H10 [24]. Mutagenesis of *ATP1* and *ATP2* genes in the two plasmids was performed using PCR. Primers used for PCR are displayed in Supplementary Material, Figure SM1. All mutants of α subunit and most mutants of β subunit were obtained by successively transforming *S. cerevisiae* cells (W303-1A-*Δatp1Δatp2 MAT a*, *ade2-1*, *his3-1,15*, *leu2-3,112*, *trp1-1*, *ura3-1*) kindly provided by Pr David Mueller (Chicago, IL, USA) with pVC2-ATP1 and pRS313/ATP2-H10 plasmids. Cells were first transformed by WT or mutated pRS313/ATP2-H10 and selected on a fermentable medium (FM) containing 0.7% Yeast Nitrogen Base without amino acids, 2% glucose, supplemented with 60 mg/L leucine, 20 mg/L adenine, 20 mg/L tryptophan and 20 mg/L uracil. Selected cells were grown in a medium containing 1% yeast extract, 1% Bacto peptone and 2% glucose. Then they were transformed with WT or mutated pVC2-ATP1 plasmid. Transformed cells were selected and grown at 30 °C on a strictly respiratory medium (RM) containing 1% yeast extract, 0.1% KH_2PO_4, 0.12% $SO_4(NH_4)_2$, and 2% lactate, supplemented with 60 mg/L leucine, 20 mg/L adenine and 20 mg/L tryptophan, pH 5.5. Each of the mutated strains was checked for its auxotrophy on the final sample used for mitochondria preparation. For double mutations β-T380R-S383E, β-E471K-A474E and the quadruple mutation β-T380R-S383E-E471K-A474E, *S. cerevisiae* cells (Euroscarf BY4741-*Δatp2 MAT a*, *his3Δ1*, *leu2Δ0*, *met15Δ0*, *ura3Δ0*, *YJR121w::kanMX4*) were transformed with the WT or the mutated pRS313/ATP2-H10 plasmid. Transformants were selected and grown at 30 °C on RM supplemented with 40 mg/L methionine, 60 mg/L leucine, 20 mg/L adenine, 20 mg/L tryptophan, 20 mg/L uracil, and 200 mg/L G418, pH 5.5.

2.2. Mutagenesis of γ subunit

γ subunit mutagenesis was achieved by PCR amplification using DNA from strain W303-1B as a template. Primers used for PCR are displayed in Supplementary Material, Figure SM1. PCR product was digested with *Hin*dIII-*Not*I and ligated into the vector pES425#1 (Doron Rapaport). All mutants of γ subunit were obtained by transforming *S. cerevisiae* cells (W303-1B *MAT α*, *ade2-1*, *his3-1,15*, *leu2-3,112*, *trp1-1*, *ura3-1*) with the pES452-γ vector and selected on FM supplemented with 20 mg/L adenine, 20 mg/L tryptophan, 20 mg/L histidine and 20 mg/L uracil. Obtained strains were subsequently deleted for *ATP3* gene with the deletion cassette of *ATP3* obtained by the PCR amplification of the pUG6 plasmid containing the KanMX4 module [28] as a template and primers displayed in Supplementary Material, Figure SM1. Transformants were selected on complete synthetic medium supplemented with 200 μg/mL G418. Transformed cells were grown at 30 °C on RM supplemented with 20 mg/L adenine, 20 mg/L histidine, 20 mg/L uracil and 20 mg/L tryptophan, pH 5.5. Each of the mutated strains was checked for its auxotrophy on the final sample used for mitochondria preparation.

2.3. Biological materials

S. cerevisiae cells were grown at 30 °C in a large volume of RM as indicated above, and cells were harvested in exponential phase to prepare mitochondria as previously described [29]. Sub-mitochondrial particles devoid of IF1 were prepared by sonication in TSE (20 mM Tris-SO_4, 200 μM EDTA, pH 8.5) as previously described [29], except that after endogenous IF1 release (4 °C, overnight) they were centrifuged for 20 min (8000 *g*, 4 °C). The supernatant was then centrifuged for 40 min (100,000 *g*, 4 °C), and the new pellet was resuspended into a small volume (100–200 μL) of TSE, then kept on ice before use. His-tagged yIF1 was overexpressed in *Escherichia coli* and the peptide was purified as previously [25] using a Ni-NTA column. The His-tag was removed using enterokinase. yIF1 produced in this work differed from the WT in two points: Phe28 was replaced by Trp to allow spectrophotometric detection of the protein at 280 nm, and the first residue (Ser) was replaced by the triplet Ala-Met-Ala, which was found to improve the purification and the stability of the peptide. None of these modifications altered the binding properties of the inhibitory peptide.

2.4. Determination of specific ATPase activity in mitochondria

Mitochondria were diluted at a concentration of 15–30 μg/mL in a stirred and thermostated spectrophotometric cuvette (25 °C) containing 0.65 M mannitol, 20 mM Tris-maleate, 3 mM potassium phosphate (pH 8.5), 1 mM $MgCl_2$, 17 mM KCl, 1 mg/mL BSA, 2 mM phosphoenolpyruvate and 0.4 mM NADH. The absorbance at 340 nm was continuously monitored. After 2 min of incubation, mitochondria were supplemented with 20 μg/mL alamethicin to rapidly permeabilize the membranes and to dilute in the medium the inhibitory peptide previously released from ATP synthase by membrane energization [29]. Then, 20 units/mL of pyruvate kinase and 50 units/mL of lactate dehydrogenase were added and the reaction was finally triggered by adding 1 mM MgATP (Figure SM2 of Supplementary Material). The rate of ATP hydrolysis was constant for several minutes. The reaction was fully inhibited by addition of IF1 at high concentration. Each experiment was performed in triplicate.

2.5. ATP synthase content determination in mitochondria

Mitochondrial proteins (25 μg) were separated *via* SDS-PAGE and probed with antibodies against the indicated proteins (Figure SM3 of Supplementary Material). SDS-PAGE was conducted as described by Laemmli [30] and by Schägger and von Jagow [31]. Western blot analyses were performed as previously described [32]. Polyclonal antibodies raised against yeast ATP synthase were used at a dilution of 1:10,000 for subunits γ, δ, Atp4p and a-Atp6p. Nitrocellulose membranes were

incubated with peroxidase-labelled antibodies at a 1:5000 dilution (Promega), and the blot visualization was conducted with ECL reagent. Data acquisition was performed using the Syngene G-Box and quantification using ImageJ software. The ATP synthase amount for every mutant was normalized to that of WT material on the basis of subunit a-Atp6p only, because the effective accumulation of this subunit is a good indication that it was assembled in ATP synthase. Subunit a-Atp6p indeed is very labile and rapidly degraded when it cannot assemble [33–35]. From duplicate experiments the precision of the mutant/wT a-Atp6p ratio was estimated to 25%. The absolute ATP synthase content of WT mitochondria was estimated by using purified F_1-ATPase as a standard, on the basis of γ subunit.

2.6. ATP hydrolysis measurement in SMP

Continuous monitoring of ATP hydrolysis by SMP coupled to NADH oxidation was carried out spectrophotometrically as described [25]. The reaction was observed in a stirred and thermostated cuvette (25 °C) containing 50 mM MES (pH 6.5) or 50 mM Tris (pH 8.0), 20 mM KCl, 1 mM $MgCl_2$, 1 mM phosphoenolpyruvate, 20 units/mL pyruvate kinase, 50 units/mL lactate dehydrogenase, 0.4 mM NADH, 1 mM MgATP unless otherwise indicated, 2 μM antimycin and 2 μM FCCP. ATP hydrolysis was initiated by adding SMP and monitored by NADH absorbance decrease at 340 nm.

Estimation of K_m for ATP hydrolysis was carried out by measuring the rate of ATP hydrolysis by SMP in the same reaction medium adjusted to pH 8.5 or 8.0, at different MgATP concentrations. Seven successive MgATP additions were performed on the same sample at sufficient time intervals to reach the steady state. This could take more than 10 min at low MgATP concentrations. The successive cumulated ATP concentrations were 10, 20, 50, 100, 200, 500 and 1000 μM (Figure SM4 of Supplementary Material). K_m was estimated by non-linear regression using MicroCal Origin software.

2.7. Kinetic analysis of ATPase activity inhibition by IF1

After some minutes of steady state ATP hydrolysis as previously indicated, yIF1 was injected and ATPase activity decayed. This decay was monoexponential and the rate constant of decay was a linear function of inhibitor concentration. This is consistent with a first-order inhibition reaction:

$$E + I \underset{k_{off}}{\overset{k_{on}}{\rightleftharpoons}} EI \qquad \text{(Scheme1)}$$

where E is active and EI inactive. The inhibition pattern and the meaning of measured kinetic constants are actually more complex than suggested by this simple model. This will be developed in Appendix A and in the Supplementary Material. The spectrophotometric recording after IF1 addition was fitted to the following function corresponding to the integral of the monoexponential decay of ATPase activity:

$$y(t) = V_{eq}t + \left[\left(V_0 - V_{eq}\right)/k_{app}\right]\left[1 - \exp\left(-k_{app}t\right)\right] + y_0 \qquad (1)$$

where $y(t)$ is the absorbance at time t, and y_0 the absorbance at zero time defined as the time of IF1 addition. V_0 is the constant rate of absorbance variation before IF1 addition in absorbance units per second (proportional to the initial ATPase activity), V_{eq} the final rate of absorbance variation after IF1 addition (proportional to the final ATPase activity), and k_{app} the apparent inhibition rate constant in s^{-1}. The obtained k_{app} value was plotted as a function of the inhibitor concentration [I] to determine the rate constants k_{on} (in $M^{-1}\ s^{-1}$) and k_{off} (in s^{-1}) according to:

$$k_{app} = k_{on}[I] + k_{off}. \qquad (2)$$

The relation between the V_{eq}/V_0 ratio and the inhibitor concentration was fitted to the following function:

$$V_{eq}/V_0 = v_r + (1 - v_r)/(1 + [I]/K_d) \qquad (3)$$

where v_r is the inhibitor-insensitive fraction of V_0 (always lower than 5%). Theoretically, K_d should be equal to the k_{off}/k_{on} ratio. k_{off} was also directly calculated using the following linear relationship between $1/k_{app}$ and V_{eq}/V_0, drawn from Eqs. (1) and (3):

$$V_{eq}/V_0 = v_r + \left[(1 - v_r)\, k_{off}\right]\left(1/k_{app}\right). \qquad (4)$$

k_{on}, K_d and k_{off} values and their standard errors were obtained by fitting the experimental data with Eqs. (2), (3) and (4), respectively, using MicroCal Origin software. In all of the experiments, the inhibitor concentration was much higher than the enzyme concentration. Therefore the total and free concentrations of inhibitor could be considered identical and constant during the kinetics of inhibition. One experiment consisted in a set of at least ten kinetics obtained with different IF1 concentrations.

2.8. Chemicals and reagents

All reagents were of analytical grade. PCR mutagenesis was carried out using the QuikChange Site-Directed Mutagenesis Kit from Stratagene (La Jolla, CA, USA). DNA ligase was from New England Biolabs (Ipswitch, MA, USA). BCIP (5-bromo-4-chloro-3-indolyl phosphate) and NBT (nitro blue tetrazolium) were from Bethesda Research Laboratories (Gaithersburg, MD, USA). Yeast extract was from Difco (Detroit, MI, USA). ATP, NADH, and phosphoenolpyruvate were purchased from Roche (Basel, Switzerland). Pyruvate kinase and lactate dehydrogenase were purchased from Sigma-Aldrich (St Louis, MO, USA).

3. Results

3.1. Classes of mutations in α and β subunits

We mutated some residues or groups of residues of the yeast ATP synthase and examined the consequences of these mutations on IF1 binding parameters. To select the amino acids to be mutated, we defined four distinct classes of residues surrounding IF1 in the crystallized IF1/F1-ATPase complexes [10,11], two located in αDP subunit (classes A and C) and two in βDP subunit (classes B and D) (Fig. 1). In each subunit, the two classes of residues were discriminated on the basis of the distance from the foot of the γ subunit. Classes A (α subunit) and B (β subunit) consist of discrete amino acids, remote from γ, generally well conserved within mitochondrial ATP synthases but not in other ATP synthases. Classes C (α subunit) and D (β subunit) are motifs of contiguous, highly conserved amino acids, some of them interact with γ. We also mutated some γ residues that interact with class C residues in the 3D crystal structure of the yeast and bovine inhibited complexes.

In this study, 19 mutants of ATP synthase were produced. Mitochondria and SMP were prepared from these mutants. In all cases, mitochondria oxidized NADH at high rates, and the respiration rate was stimulated by ADP and by FCCP (not shown). We more especially estimated the effect of the mutations on the catalytic properties of ATP synthase. To achieve this goal, we first determined the maximal catalytic capacity of mitochondria by measuring the rate of ATP hydrolysis (1 mM MgATP) at pH 8.5, after a brief membrane pre-energization followed by alamethicin addition. This treatment results in fast and full release of the inhibitory peptides IF1 and STF1 [29]. As compared to SMP preparation, it has the advantage to avoid losses of activity. In a second step, to convert the maximal specific activity into the maximal catalytic turnover of the enzyme, we estimated the ATP synthase content of mitochondria by immunological titration. Finally, we determined the K_m for ATP on SMP by measuring the rate of ATP hydrolysis at different MgATP concentrations, at pH 8.5 and pH 6.5. SMP was here

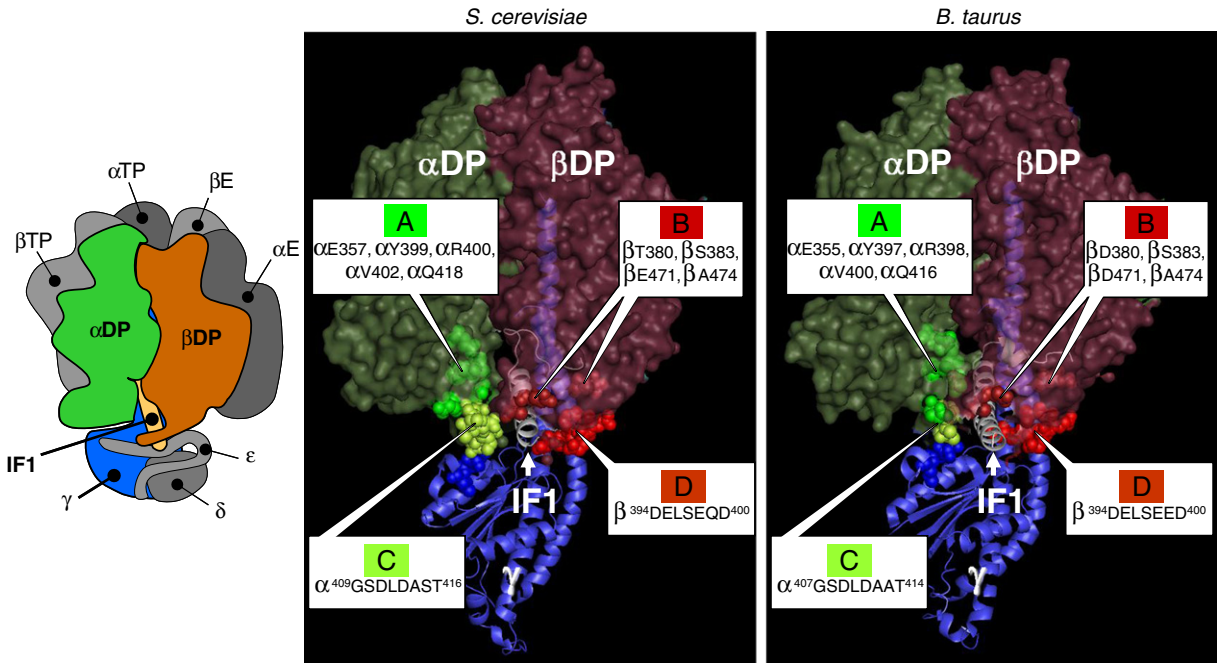

Fig. 1. Mutated residues in the yeast F_1-ATPase inhibited with IF1 and corresponding residues in the bovine species. Left image, *S. cerevisiae* model, pdb entry *3zia*; only residues 1–36 of IF1 were solved. Right image, *B. taurus* model, pdb entry *2v7q*; only residues 8–50 of truncated IF1 containing residues 1–60 were solved. Image created using PyMol software. Only αDP, βDP, γ and IF1 are represented for the sake of clarity. A, B, group of discrete residues remote from the foot of γ subunit; A, residues located on αDP subunit, close to the catalytic interface entrapping IF1 midpart; B, residues located on βDP subunit, close to the N-extremity or to the midpart of IF1; C, D, groups of contiguous residues close to the foot of γ subunit, only a part of which are close to IF1; C, residues located on αDP subunit; D, residues located on βDP subunit. The topological arrangement of all F_1-ATPase subunits is recalled by the scheme on the left side of the figure. Nomenclature of catalytic interfaces (DP, TP, E) is defined by their nucleotide occupancy in the reference 3D structural model [12], see Introduction for details.

preferred to alamethicin-permeabilized mitochondria because activity measurements are simpler and K_m determination is independent of the amount of active enzymes. Table 1 shows that the mutations diminished the maximal catalytic turnover of the enzyme and altered the K_m value to various extents. The possible consequences of these changes on IF1 binding mechanism will be examined in the Discussion section.

3.2. IF1 binding parameter estimates and meaning

The kinetics of inhibition by IF1 was studied only using SMP. The rate constant of association k_{on} is related to the recognition step, whereas thermodynamic and kinetic constants of dissociation, K_d and k_{off}, are inversely related to the stability of the inhibited complex. Fig. 2 shows typical examples of determination of these constants from single experiments. Importantly, the k_{off} value was not only here estimated by the $K_d k_{on}$ product as in previous studies [25,26,11], but also by directly correlating the residual activity at equilibrium to $1/k_{app}$ (see Materials and methods, Eq. (4)). This makes k_{off} determination insensitive to possible uncertainties on IF1 concentrations. Comparison of these two k_{off} values allows evaluating self-consistency, and then reliability of parameter estimates. Fig. 2 shows an example of single experiments from three phenotypes in which the $k_{off}/K_d k_{on}$ ratios are 1.6 ± 1.2, 1.4 ± 0.5 and 1.05 ± 0.26. These values are reasonably close to the theoretically expected ratio of 1.

It has been previously shown that the measured association rate constant k_{on} of IF1 depends on MgATP concentration [36], because it is actually modulated by the nucleotide occupancy and the catalytic turnover of F_1-ATPase [23,24]. This has been studied in the case of isolated F_1-ATPase and can be also observed here in the case of SMP. Fig. 3a shows the k_{app} value as a function of MgATP concentration with a single IF1 concentration (75 nM). Because IF1 concentration is constant here, k_{app} is directly related to k_{on} [see Eq. (2)]. The sharp rise of k_{on} with MgATP concentration in the μM range can be explained by a turnover-dependent competition between release and locking of loosely bound IF1 [23,24]. A moderate decrease of k_{on} is observed at high MgATP concentrations. It probably means that increasing nucleotide occupancy of catalytic sites slows down the loose binding of IF1. A kinetic model supporting this view is briefly presented in Appendix A and extensively developed in the Supplementary Material. At 1 mM MgATP concentration the k_{on} value reaches a plateau and is likely to represent the true rate binding constant of IF1 to the enzyme saturated with substrate. For this reason, experiments reported in the following of our study were carried out with 1 mM MgATP.

Since the apparent k_{on} value depends on the catalytic state of the enzyme, one may wonder if it is also the case for k_{off}. Fig. 3b shows that the residual activity at equilibrium and k_{on} value vary symmetrically to each other over MgATP concentration. In Fig. 3c the residual activity is plotted as a function of $1/k_{app}$. The relationship between the two values is grossly linear, as expected if k_{off} is constant at all MgATP concentrations (see Eq. (4)). On the same graph, we have also plotted the values obtained at a constant MgATP concentration (1 mM) but with variable concentrations of IF1, as in Fig. 2c. The two plots are not very different. k_{off} value is 23.8 ± 2.6 s^{-1} with variable IF1 concentration and 33.2 ± 2.0 s^{-1} with variable MgATP concentration. This indicates that contrary to k_{on}, k_{off} is practically constant when MgATP concentration varies from 0.1 μM to 1 mM. This result corroborates early experiments in which the rate of release of radiolabelled IF1 from energized ox-heart SMP has been shown to be independent of MgATP concentration [21].

3.3. Effect of mutations of γ-remote residues

The residues of classes A and B were selected on the basis of two criteria: their proximity of IF1 in crystals and their relative specificity to mitochondrial F_1-ATPases (Figure SM5 of Supplementary Material). This second criterion was applied in order to identify the residues that are responsible for the specific inhibition of mitochondrial ATP synthases by IF1 *in vitro*. IF1 peptides purified from *B. taurus* and *S. cerevisiae* indeed non-specifically inhibit F_1-ATPase from both species, but they do not inhibit F_1-ATPase from *E. coli* [37]. Accordingly, purified yIF1 does not inhibit F_1-ATPase from *PS3 bacillus* and from spinach chloroplasts, even

Table 1
Effect of mutations on catalytic properties of ATP synthase. Conditions as described under Materials and methods. Column 1, ATPase activity of mutant mitochondria permeabilized by alamethicin (pH 8.5) normalized to the activity of WT mitochondria at the same protein concentration. The activity of WT mitochondria is 2.92 ± 0.58 μmol ATP hydrolyzed per min and per mg of mitochondrial protein. Column 2, ATP synthase content of mutated mitochondria normalized to the content of WT mitochondria at the same total protein concentration. This content was calculated from immunological staining of subunit a-Atp6p. Column 3, ratio between the catalytic turnovers of mutated and WT ATP synthases, obtained by dividing numbers of column 1 by numbers of column 2. The absolute ATP synthase content of WT mitochondria was estimated from immunological staining of γ subunit using purified F_1-ATPase as a standard. The F_1 subcomplex was thus estimated as 6% of the total mass protein in WT mitochondria. From this measurement and from the specific activity of wT mitochondria, the catalytic turnover of WT ATP synthase at pH 8.5 was estimated to about 300 s^{-1}. Columns 4 and 5, Michaelis constant for ATP hydrolysis (K_m) at pH 8.5 and at pH 6.5, determined using SMP.

Mutation	Activity pH 8.5	F_0F_1 content	Catalytic turnover pH 8.5	K_m (μM)	
	(rel. to WT)	(rel. to WT)	(rel. to WT)	pH 8.5	pH 6.5
None (WT)	1	1	1	63 ± 4	42 ± 3
Class A					
α-E357D-Y399F-R400A-V402L-Q418N	0.58 ± 0.07	2.0 ± 0.5	0.3 ± 0.1	274 ± 30	76 ± 7
Class B					
β-T380R-S383E	0.88 ± 0.17	1.9 ± 0.5	0.5 ± 0.2	74 ± 7	32 ± 2
β-E471K-A474E	1.06 ± 0.13	0.9 ± 0.2	1.2 ± 0.5	51 ± 2	28 ± 1
β-T380R-S383E-E471K-A474E	0.84 ± 0.02	0.9 ± 0.2	0.9 ± 0.2	62 ± 3	34 ± 1
Class C					
α^{409}GS**G**LDAST^{416}	0.30 ± 0.10	1.3 ± 0.3	0.2 ± 0.1	141 ± 4	49 ± 6
α^{409}GSD**L**GAST^{416}	0.17 ± 0.01	1.0 ± 0.3	0.2 ± 0.1	89 ± 3	37 ± 5
α^{409}GS**GL**GAST^{416}	0.50 ± 0.03	1.8 ± 0.5	0.3 ± 0.1	152 ± 2	105 ± 2
α^{409}GS**GGG**AST^{416}	0.93 ± 0.05	0.6 ± 0.2	1.5 ± 0.5	89 ± 8	87 ± 5
α^{409}G**GGGG**AST^{416}	0.85 ± 0.01	1.1 ± 0.3	0.8 ± 0.2	137 ± 5	99 ± 6
α^{409}GS**GGGGGG**^{416}	0.54 ± 0.02	1.4 ± 0.4	0.4 ± 0.1	82 ± 2	69 ± 2
α^{409}G**GGGGGGG**^{416}	0.67 ± 0.08	1.6 ± 0.4	0.4 ± 0.2	76 ± 8	65 ± 3
α^{409}GS - - - AST^{416}	0.67 ± 0.05	0.6 ± 0.1	1.2 ± 0.4	78 ± 4	46 ± 5
Class D					
β^{394}**G**ELSEQD^{400}	0.54 ± 0.02	1.6 ± 0.4	0.3 ± 0.1	59 ± 2	29 ± 3
β^{394}D**G**LSEQD^{400}	0.84 ± 0.04	0.9 ± 0.2	0.9 ± 0.3	63 ± 14	61 ± 3
β^{394}DELS**G**Q**G**^{400}	0.59 ± 0.02	1.7 ± 0.4	0.4 ± 0.1	70 ± 3	36 ± 2
β^{394}D**GGG**EQD^{400}	0.58 ± 0.04	1.5 ± 0.4	0.4 ± 0.1	66 ± 4	44 ± 6
Classes C–D					
α^{409}GS - - - AST^{416} β^{394}D**G**LSEQD^{400}	0.40 ± 0.02	2.3 ± 0.6	0.2 ± 0.1	85 ± 4	68 ± 10
γ					
γ-M116G-Q117G	0.64 ± 0.01	1.9 ± 0.5	0.4 ± 0.1	56 ± 3	37 ± 2
γ-M116G-Q117G-L118G	0.61 ± 0.05	2.3 ± 0.6	0.3 ± 0.1	105 ± 13	51 ± 12

after removal of the chloroplastic ε subunit (Figure SM6 of Supplementary Material).

The selected residues were mutated into their non-mitochondrial counterparts (Figure SM5). All α-subunit residues (E357, Y399, R400, V402, Q418) and two β-subunit residues (T380, S383) were mutated into the residues present in almost all chloroplastic sequences and in a number of bacterial sequences. βE471 and βA474, located in a region poorly conserved in the non-mitochondrial world, were respectively mutated into their *E. coli* and chloroplastic homologues. At saturating concentration, IF1 inhibits ATPase activity to more than 95% in SMP prepared from all these mutants. Binding parameters were obtained after merging the results of several independent kinetic experiments as those displayed in Figs. 2, 3–4 experiments for mutants, and 29 experiments for WT. Results obtained at pH 6.5 are displayed in Table 2. Fig. 4a

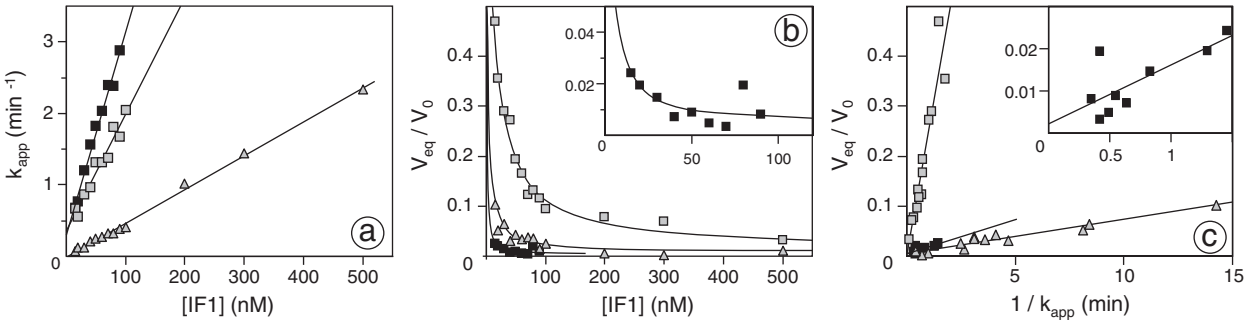

Fig. 2. Kinetic data of IF1 inhibition from single typical experiments carried out with SMP from three different cell lines and determination of binding parameters. Conditions as described under Materials and methods, pH 6.5. (-■-) WT; (-□-) α-Δ[D411-L412-D413]; (-△-) β-E471K-A474E. Panel a, rate constant of inhibition (k_{app}) as a function of IF1 concentration, for k_{on} determination. Panel b, normalized ATPase activity at equilibrium as a function of IF1 concentration, for K_d determination. Panel c, normalized ATPase activity at equilibrium as a function of $1/k_{app}$, for k_{off} determination. Enlarged view of WT data is displayed in b and c. Resulting parameters: WT, $k_{on} = (4.7 \pm 0.3)\ 10^5\ M^{-1}\ s^{-1}$, $K_d = (3.0 \pm 1)\ 10^{-10}$ M, $k_{off} = (2.3 \pm 0.8)\ 10^{-4}\ s^{-1}$, $k_{off}/K_d k_{on} = 1.6 \pm 1.2$; α-Δ[D411-L412-D413], $k_{on} = (2.2 \pm 0.6)\ 10^5\ M^{-1}\ s^{-1}$, $K_d = (1.18 \pm 0.08)\ 10^{-8}$ M, $k_{off} = (3.6 \pm 0.3)\ 10^{-3}\ s^{-1}$, $k_{off}/K_d k_{on} = 1.4 \pm 0.5$; β-E471K-A474E, $k_{on} = (7.9 \pm 0.2)\ 10^4\ M^{-1}\ s^{-1}$, $K_d = (1.4 \pm 0.2)\ 10^{-9}$ M, $k_{off} = (1.1 \pm 0.1)\ 10^{-4}\ s^{-1}$, $k_{off}/K_d k_{on} = 1.05 \pm 0.26$. The $k_{off}/K_d k_{on}$ ratio should theoretically be 1.

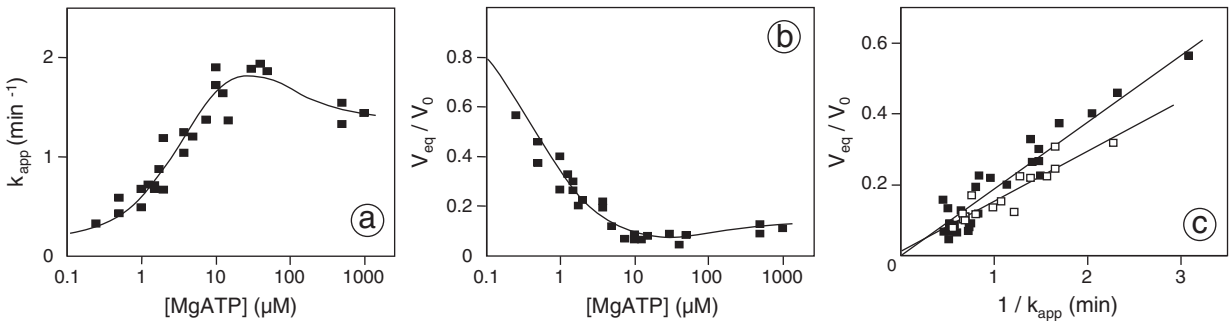

Fig. 3. Effect of MgATP concentration on IF1 rate constants of association and dissociation. Conditions as described under Materials and methods. pH 8, SMP from wT cell line, merged data from two experiments. Panel a, rate constant of inhibition (k_{app}) as a function of MgATP concentration (log scale) with a fixed IF1 concentration (75 nM). Panel b, normalized ATPase activity at equilibrium as a function of MgATP concentration. Panel c, normalized ATPase activity at equilibrium as a function of $1/k_{app}$, for k_{off} determination. (-■-) variable Mg concentration, data replotted from panel a, $k_{off} = (33.2 \pm 2.0)\ 10^{-4}\ s^{-1}$. (−□−) variable IF1 concentration, same SMP samples, $k_{off} = (23.8 \pm 2.6)\ 10^{-4}\ s^{-1}$. Data in panel a were fitted to the model presented in Appendix A using Eqs. (A1) and (A2) and fixed values for k_{off} and K_m. k_{off} value was determined from panel c and K_m value was estimated to 46.3 μM from the relationship between MgATP concentration and the steady state rate of ATP hydrolysis (data not shown). The following parameters were deduced from the fit: $k^A_{on} = (5.8 \pm 0.7)\ 10^5\ M^{-1}\ s^{-1}$, $k^B_{on} = (3.0 \pm 0.3)\ 10^5\ M^{-1}\ s^{-1}$, $k_{lock}/k_{off} = (8.4 \pm 2.0)\ s^{-1}$.

focuses on the values of IF1 association and dissociation rate constants, the latter being estimated by k_{off} as well as by the K_dk_{on} product (see Materials and methods and Section 3.2). Combined mutagenesis of the five residues selected on α (class A) had no effect on the binding rate constant k_{on}. It increased the rate constant of dissociation or had no significant effect, depending whether it is determined by k_{off} or by the product K_dk_{on}. On the β subunit (class B), the double mutation T380R-S383E had no significant effect on k_{on} value and the double mutation β-E471K-A474E decreased the k_{on} value by a factor of 7. Combining the four mutations has no significant additional effect as compared to E471K-A474E. Mutations on the β subunit had no significant effect on the dissociation rate constant.

To further define the effects of the mutations on the dissociation rate constant, we did some complementary experiments at pH 8 for which this constant is higher. At this pH, the K_d value of WT dramatically increased from 0.24 nM to 9 nM, the k_{off} value from $1.8\ 10^{-4}\ s^{-1}$ to $1.8\ 10^{-3}\ s^{-1}$, and the K_dk_{on} product from $0.9\ 10^{-4}$ to $2\ 10^{-3}\ s^{-1}$, which almost perfectly matches the k_{off} value. Binding constant values at pH 8 are displayed in Table 3 and k_{on}, k_{off} and K_dk_{on} are shown in Fig. 4b. It is confirmed that the quintuple mutation on α subunit had no effect on k_{on}, whereas it increased the k_{off} value and the K_dk_{on} product by about 2.5 fold. The double mutation β-E471K-A474E or the quadruple mutation β-T380R-S383E-E471K-A474E actually increased by a factor of 2 to 2.5 the dissociation rate constant estimated either by k_{off} or by K_dk_{on}, whereas the double mutation β-T380R-S383E had no effect.

3.4. Effect of mutations of α subunit residues close to the foot of γ subunit

This region of α subunit was chosen for mutagenesis because in the α subunit in DP state it interacts with the foot of the γ subunit. This interaction does not exist in the bovine non-inhibited complex (pdb files *1bmf*, *1e79* and *2jdi*). So we felt that it might contribute to the inhibitory effect of IF1, but indirectly. We studied IF1 binding parameters after mutation into glycine of an increasing number of residues of the ^{409}GSDLDAST^{416} motif. Results are displayed in Table 2 (class C), and Fig. 5 focuses on the values of IF1 association and dissociation constants.

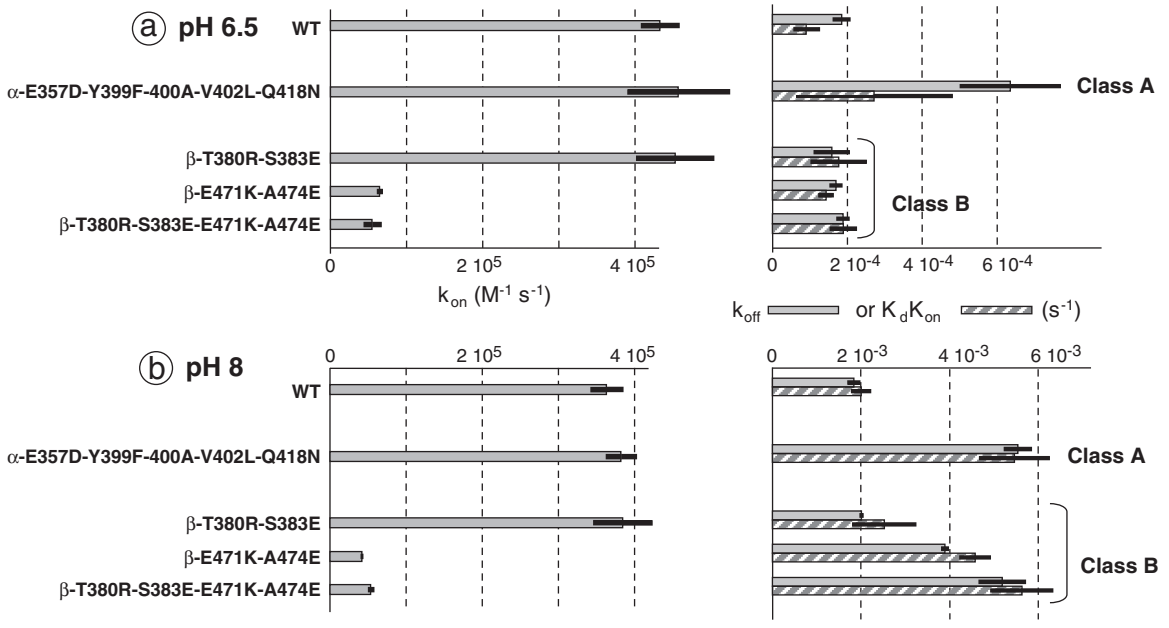

Fig. 4. Kinetic constants of IF1 binding and release after mutagenesis of group A and group B residues. (a), pH 6.5; (b), pH 8. The dissociation constant is expressed by k_{off} (grey bars) or by the product K_dk_{on} (hatched bars). Standard deviation is indicated by thin black bars. The effects of mutations on k_{on} are similar at pH 6.5 and pH 8. The effect on k_{off} and K_dk_{on} appears more consistent at pH 8 than at pH 6.5 (see text for details).

Table 2
IF1 binding parameters at pH 6.5 with ATP synthase mutated on α and β subunits. Experimental conditions and calculations as described under Materials and methods, pH 6.5. n, number of experiments.

Mutation	k_{on} (10^5 M^{-1} s^{-1})	K_d (10^{-9} M)	k_{off} (10^{-4} s^{-1})	K_dk_{on} (10^{-4} s^{-1})	n
None (WT)	4.3 ± 0.2	0.24 ± 0.06	1.8 ± 0.2	0.9 ± 0.3	29
Class A					
α-E357D-Y399F-R400A-V402L-Q418N	4.6 ± 0.7	0.6 ± 0.4	6.4 ± 1.3	2.8 ± 2.0	3
Class B					
β-T380R-S383E	4.5 ± 0.5	0.4 ± 0.1	1.6 ± 0.5	1.8 ± 0.7	3
β-E471K-A474E	0.64 ± 0.02	2.2 ± 0.2	1.7 ± 0.2	1.4 ± 0.2	4
β-T380R-S383E-E471K-A474E	0.5 ± 0.1	3.5 ± 0.4	1.9 ± 0.2	1.9 ± 0.5	3
Class C					
α^{409}GS**G**LDAST^{416}	2.3 ± 0.2	1.3 ± 0.2	3.0 ± 0.2	3.0 ± 0.7	3
α^{409}GSDL**G**AST^{416}	3.6 ± 0.5	0.6 ± 0.2	4.7 ± 0.6	2.2 ± 1.0	3
α^{409}GS**GLG**AST^{416}	1.7 ± 0.2	10.0 ± 1.0	9.8 ± 1.7	17.0 ± 4.0	3
α^{409}GS**GGG**AST^{416}	1.7 ± 0.2	13.7 ± 1.4	24.4 ± 1.9	23.3 ± 5.8	3
α^{409}G**GGGG**AST^{416}	1.7 ± 0.2	6.0 ± 1.4	16.6 ± 4.3	10.2 ± 3.9	4
α^{409}GS**GGGGGG**^{416}	1.6 ± 0.1	14.7 ± 2.0	31.1 ± 4.0	23.5 ± 4.4	4
α^{409}G**GGGGGGG**^{416}	2.8 ± 0.2	5.5 ± 0.2	15.6 ± 1.3	15.4 ± 1.7	3
α^{409}GS - - - AST^{416}	2.5 ± 0.2	16.8 ± 3.0	50 ± 12	42 ± 11	4
Class D					
β^{394}**G**ELSEQD^{400}	4.0 ± 0.3	0.8 ± 0.2	5.0 ± 0.7	3.2 ± 1.1	3
β^{394}D**G**LSEQD^{400}	5.7 ± 0.4	2.7 ± 0.2	18.6 ± 2.4	15.4 ± 2.5	3
β^{394}DELS**G**QG^{400}	3.8 ± 0.4	1.1 ± 0.4	6.0 ± 0.6	4.2 ± 1.8	3
β^{394}D**GGG**EQD^{400}	3.9 ± 0.8	0.4 ± 0.3	3.8 ± 0.8	1.6 ± 1.4	3
Classes C–D					
α^{409}GS - - - AST^{416} β^{394}D**G**LSEQD^{400}	nd	193 ± 18	nd	nd	4

Mutations into glycine resulted in moderate decrease of the k_{on} value and in more pronounced decrease of IF1 affinity. The dissociation rate constant gradually increases with the number of mutated residues, except when S410 is replaced by G. This mutation results in a small decrease of k_{off}, as it can be seen by comparing ^{409}G**GGGG**AST^{416} to ^{409}GS**GGG**AST^{416} and ^{409}G**GGGGGG**^{416} to ^{409}GS**GGGGG**^{416}. The highest k_{off} value was obtained after mutating 6 amino acids into glycine. It reached about 3 10^{-3} s^{-1}, *i.e.* 15–30 times the value obtained with the WT. Another mutation, consisting in removing the three amino acids α-D411, α-L412 and α-D413, had a higher effect on the dissociation rate constant (k_{off} = 5 10^{-3} s^{-1}).

Globally, except for S410G mutation, decreasing the steric hindrance of the α^{409}GSDLDAST^{416} motif tends to destabilize the inhibited IF1-F_1ATPase complex. In the αDP subunit of the crystallized yeast IF1-ATPase complex, ^{409}GSDLDAST^{416} amino acids face ^{116}MQLL^{119} residues belonging to an α-helix of the γ subunit. In particular, αD411, αL412 and αD413 are closer to the γ^{116}MQLL^{119} motif than to IF1 (Fig. 1). This suggests that k_{off} increase consecutive to their mutation or deletion could be due, at least in part, to modifications of αDP-γ interactions in this region. In this case, diminishing the steric hindrance of the γ^{116}MQLL^{119} motif is also expected to increase k_{off}. We have then performed the double mutation γ-M116G-Q117G and the triple mutation γ-M116G-Q117G-L118G. We examined their effect on IF1 binding. Not surprisingly, these mutations had no effect on the k_{on} value. The double mutation γ-M116G-Q117G resulted in increasing the k_{off} value by more than 70%, a limited but significant effect observed both at pH 6.5 and at pH 8. At pH 8, the k_{off} value shifted from 1.8 10^{-3} s^{-1} (WT) to 3.1 10^{-3} s^{-1} (γ-M116G-Q117G). The triple mutation γ-M116G-Q117G-L118G restored k_{off} to the wild type value. Results obtained at pH 8 are detailed in Table 3 and in Fig. 6.

Taken together, these results show that modifications in the α–γ contact region involving ^{409}GSDLDAST^{416} and γ-^{116}MQLL^{119} affect the dissociation rate constant and the affinity of the peptide for the enzyme. The effect of the double mutation γ-M116G-Q117G is limited and reversed

Table 3
IF1 binding parameters at pH 8 with ATP synthase mutated on α, β and γ subunits. Experimental conditions and calculations as described under Materials and methods. n, number of experiments.

Mutation	k_{on} (10^5 M^{-1} s^{-1})	K_d (10^{-9} M)	k_{off} (10^{-4} s^{-1})	K_dk_{on} (10^{-4} s^{-1})	n
None (WT)	2.2 ± 0.1	9.1 ± 0.6	18.4 ± 1.3	20.0 ± 2.0	7
Class A					
α-E357D-Y399F-R400A-V402L-Q418N	2.3 ± 0.2	23.4 ± 2.2	55.5 ± 7.8	54.6 ± 7.8	1
Class B					
β-T380R-S383E	2.3 ± 0.2	10.8 ± 2.0	20.1 ± 0.3	25.3 ± 7.1	1
β-E471K-A474E	0.25 ± 0.01	182 ± 10	39.0 ± 0.6	45.5 ± 3.4	1
β-T380R-S383E-E471K-A474E	0.32 ± 0.02	173 ± 12	52.0 ± 5.2	55.4 ± 6.9	1
γ subunit					
γ-M116G-Q117G	2.2 ± 0.1	19.8 ± 1.5	30.9 ± 0.8	42.6 ± 5.3	5
γ-M116G-Q117G-L118G	2.6 ± 0.1	9.00 ± 0.6	21.2 ± 0.8	23.0 ± 2.5	3

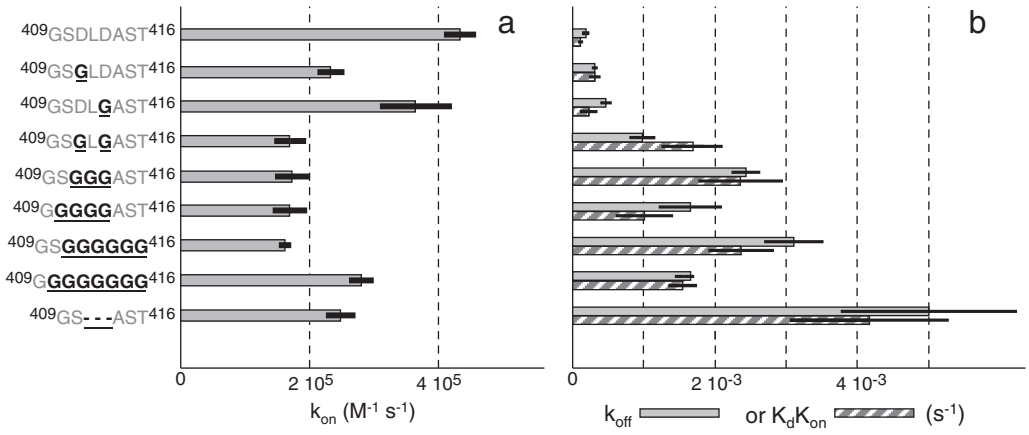

Fig. 5. Kinetic constants of IF1 binding and release after mutagenesis of group C residues. Data from Table 3. Mutated or deleted residues are indicated by black, bold, underlined characters. The WT sequence is GSDLDAST. Panel b, dissociation rate constant expressed by k_{off} (grey bars) or by the product K_dk_{on} (hatched bars). These two different estimates are reasonably equivalent within the experimental errors. Standard deviation is indicated by thin black bars.

by the additional γ-L118G mutation, but it remains consistent with a contribution of this α-γ contact in stabilization of the IF1-inhibited complex.

3.5. Effect of mutations of β subunit residues close to the foot of γ subunit

DELSEED (^{394}DELSEQD^{400} in yeast) is a well-conserved motif of β subunit, which periodically interacts with γ subunit during catalytic turnover [38]. Without being essential, it is involved in coupling catalysis to γ subunit rotation [39–41] and has been proposed to play a role in the inhibitory effect of the bacterial regulatory ε subunit [42], the counterpart of the mitochondrial δ subunit. Like αDP-^{409}GSDLDAST^{416}, βDP-^{394}DELSEQD^{400} is located in a region close to the foot of the γ subunit. Table 2 (class D) shows IF1 binding parameters of ATP synthase in which different residues of DELSEQD have been mutated into glycine. These mutations had no effect on the IF1 binding rate constant. All the mutations increased the dissociation rate constant. The most important increase (10–15 fold) was by far obtained with the αE395G mutation, suggesting a specific role for E395. This effect was partly reversed by the additional double mutation αL396G-αS397G.

We also combined the two mutations α-^{409}GS - - - AST^{416} and β-^{394}D**G**LSEQD^{400} which had separately the greatest effect on K_d and k_{off}. The double mutation resulted in a dramatic decrease of IF1 affinity. Minimum IF1 concentrations required to obtain significant inhibition were so high that the equilibrium between active and inhibited forms of the enzyme was reached in a few seconds. As a consequence, the inhibition could not be kinetically solved here and k_{on} could not be estimated. Only the final levels of inhibition could be estimated, which gave a K_d value of almost 200 nM (Table 2, classes C–D). This additive effect of mutations on α and β subunits illustrates the fact that multiple interactions contribute to the binding energy.

4. Discussion

4.1. Rationale

The approach developed here, a combination of site-directed mutagenesis and kinetic experiments, allows identifying domains of ATP synthase involved in initial and late steps of IF1 binding process. Previous reports only mention the effect of IF1 modifications on its binding properties [43–46,25,26,11] and a few of them include kinetic studies [25,26,11]. Here, for the first time, the effects of mitochondrial ATP synthase mutations on IF1 binding kinetics have been reported.

Residues to be mutated were initially selected on the basis of distances between their bovine homologues and IF1 in the IF1/F_1-ATPase crystallized complex (pdb file *2v7q*). The recently published structure of the equivalent yeast complex (pdb file *3zia*) has revealed some differences with the bovine structure, which will be discussed below. The γ-remote residues of α and β subunits were also selected considering their potential importance for the specific sensitivity of mitochondrial F_1-ATPases to IF1. In the case of other F_1-ATPases inhibitors indeed, specificity depends on critical residues. For example, functional experiments revealed that the aurovertin-sensitivity of mitochondrial and *E. coli* F_1-ATPases was due to a single β subunit residue [47], which was confirmed by structural data [48]. The tentoxin-sensitivity of chloroplast and *PS3 bacillus* F_1-ATPases [49] is determined by a few residues of α and β subunits [50,51]. The case of IF1 appears more complex since the mutations of the γ-

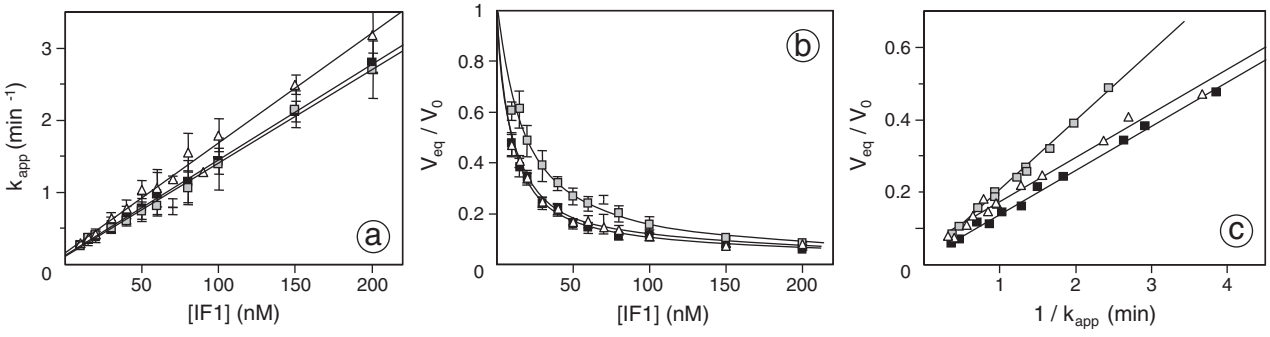

Fig. 6. Binding parameters obtained at pH 8 with SMP from wT and γ subunit mutants. Conditions as described under Materials and methods. Averaged data from at least three different experiments. (-■-) wT; (-□-) γ-M116G-Q117G; (-Δ-) γ-M116G-Q117G-L118G. Panel a, rate constant of inhibition (k_{app}) as a function of IF1 concentration, for k_{on} determination. Panel b, normalized ATPase activity at equilibrium as a function of IF1 concentration, for K_d determination. Panel c, normalized ATPase activity at equilibrium as a function of $1/k_{app}$, for k_{off} determination. Consistency of K_dk_{on} and k_{off} determinations expressed by the k_{off}/K_dk_{on} ratio: wT, 0.92 ± 0.16; γ-M116G-Q117G, 0.72 ± 0.11; γ-M116G-Q117G-L118G, 0.92 ± 0.13.

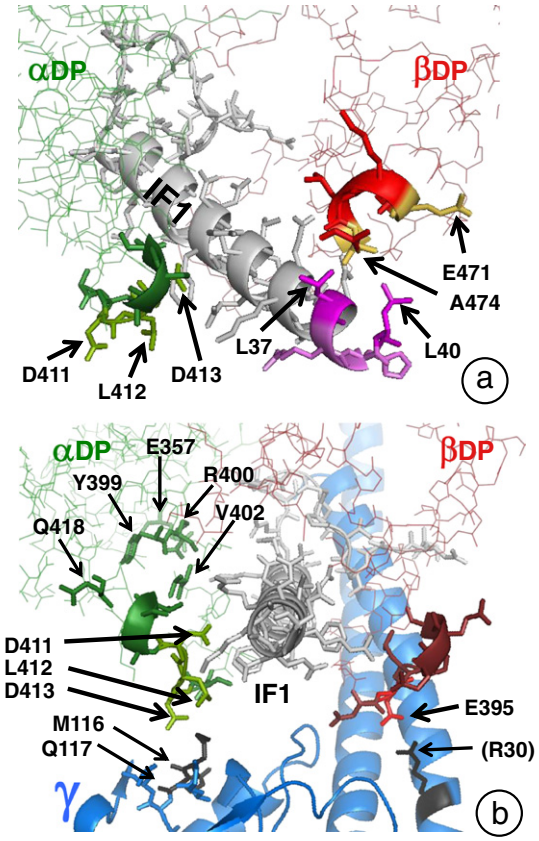

Fig. 7. Yeast F_1-ATPase motifs or residues involved in IF1 recognition and locking. Images created from the pdb file *3zia* using PyMol software. IF1 (residues 1–36, shown in grey sticks and ribbon) is mainly located between αDP (green) and βDP (red) subunits. Panel a, IF1 residues 37–40, not visible in yeast structure, were added according to the homologous bovine structure (magenta sticks and ribbon) to show the possible proximity to βDP-E471, A474 (orange sticks). Highlighted motifs in both αDP and βDP subunits are implicated in IF1 recognition step. βDP-E471, A474 play a more important role than motif α-^{409}GSDLDAST^{416} (green sticks and ribbon), in which D411, L412 and D413 have the main contribution. Panel b, γ subunit appears in blue. The motif α-^{409}GSDLDAST^{416} (green sticks and ribbon) and the motif β-^{394}DELSEQD^{400} (dark red sticks, E395 in light red), located on left and right side of IF1, respectively, play the major role in IF1 locking step. The group of residues αDP-E357-Y399-R400-V402-Q418 (green sticks) has a less important contribution, as well as βE471, A474 represented in Panel a. Highlighted residues M116, Q117 in γ subunit (black sticks) participate indirectly in IF1 locking through the possible interaction with α-^{409}GSDLDAST^{416}. Similarly, γ-R30 (black stick, residue not mutated) could contribute to IF1 locking through the potential interaction with β-^{394}DELSEQD^{400}.

remote residues into their non-mitochondrial counterparts had limited effects.

4.2. F_1-ATPase motifs or residues implicated in IF1 recognition

In initial binding step IF1 is recognized by one of the α/β catalytic interfaces which has a different conformation from that freezed in the dead-end inhibited complex (αβDP). With this restriction in mind, locations of the different residues shown to be implicated in this step are visualized in Fig. 7a (yeast IF1/F_1-ATPase complex, pdb entry *3zia*).

In β subunit the C-terminal extremity (E471, A474) is clearly involved in the initial binding step. By contrast, neither the couple of residues T380 and S383 located in the α-helix preceding β-DELSEQD, nor the β-DELSEQD motif itself is involved in IF1 recognition. On the peptide side, it is also interesting to wonder which residues might be implicated. In the bovine F_1-ATPase crystallized complex with bound IF1, residues E471 and A474 of βDP are close to residues L42, L45 and K46 of IF1, whereas in the yeast complex the homologous region of IF1 is not visible. Interestingly, mutation into alanine of yeast IF1-L40, the homologue of bovine IF1-L45, has been recently shown to decrease k_{on} by a factor of 5 [11]. This matches the 7-fold decrease of k_{on} observed here for the double mutation βE471K-βA474E. It therefore strengthens the idea that interaction between the β C-terminal extremity and IF1 midpart, presumably IF1-L40 or its neighbours, is involved in the recognition step.

In α subunit the GSDLDAST motif also seems implicated in IF1 recognition, but much less than the C-terminal extremity of β subunit. Although not really close to IF1 in the yeast crystal, αD411 residue of αDP subunit seems to have the main contribution. It should be mentioned that interactions involved in recognition might be transient, and not present in the dead-end inhibited state thought to be that of the crystallized complex. Finally, αDP subunit residues bordering IF1 midpart (αE357, αY399, αR400, αV402, αQ418) do not play any role in initial binding step.

We found that among the residues we have mutated, those playing the major role in IF1 recognition belong to the C-terminal extremity of β subunit. This part of β protrudes from the complex regardless the catalytic state of the interface. This is a facility in IF1 grasping.

4.3. Effect of mutations on k_{on} and on the catalytic properties of ATP synthase

The apparent value of k_{on} depends on the catalytic turnover rate (Fig. 3). One may then suspect that mutations indirectly change the k_{on} value, by modifying ATP synthase catalytic activity. Table 1 shows that in the case of the mutation βE471K-βA474E, which has the most pronounced effect of k_{on} (7–10 fold decrease), the maximum turnover rate is not significantly affected and the K_m value is only slightly modified. Therefore an indirect effect can here be ruled out. On the other hand, some other mutations (class A, class D, residues βT380, βS383, γM116, γQ117 and γL118) significantly decrease the catalytic activity without affecting k_{on} at all.

In class C mutants, decrease of k_{on} and catalytic activity is observed. The decrease of activity might be at least in part responsible for the k_{on} decrease. However, there is no apparent relationship, within this group, between the two effects (compare Tables 1 and 2).

To summarize, the effects of mutations on k_{on} do not seem to be the consequence of modifications of the catalytic turnover. This is particularly obvious for the couple βE471-βA474. The consequences of mutation of these residues on k_{on} value can therefore be attributed without ambiguity to the modification of their interactions with IF1 during the first step of IF1 binding.

4.4. F_1-ATPase motifs or residues implicated in the inhibited complex stabilization

After the loose IF1 binding step [23,24], the enzyme still rotates for a fraction of turn. Subunit–subunit interactions within F_1-ATPase and IF1-F_1 interactions are modified and this leads to the final inhibited state. In β subunit, the C-terminal extremity (E471, A474) poorly contributes to stabilize the inhibited complex. The DELSEQD motif of β subunit, and more especially E395, has a more significant contribution on the basis of the k_{off} increase resulting from mutations. This result needs to be related to the crystallized yeast IF1-inhibited F_1-ATPase complex (Fig. 7b), in which βDP-IF1, βTP-IF1, βDP-γ and βTP-γ interactions can be described. E395 of βDP subunit does not interact with IF1, because it is 9 Å distant from the closest IF1 residue. On the other hand, the lateral chain of βDP-E395 closely interacts with γ subunit, with distances lower than 3 Å. βDP-E395 may establish a salt bridge with γ-R30 and attractive electrostatic interactions with γ-R30 and γ-K81. In the βTP subunit (not visible in Fig. 7b), the only IF1 residue located in the neighbouring of E395 is R20, with a distance higher than 4.7 Å. βE398 also contributes, to a lower extent, to stabilize the inhibited complex. In βDP, the lateral chain of E398 may establish a salt bridge with IF1-R32, and βTP-E398 makes a H-bond with γ-Q117. Overall, β-DELSEQD motif residues that contribute

the most to IF1 locking interact more with the γ subunit than with IF1 in the crystallized complex.

In α subunit, the GSDLDAST motif has a sizeable role in the inhibited complex stability. Except for a possible hydrophobic interaction between αL412 and IF1-F27 (distance 4.2 Å) and a possible electrostatic interaction between αD413 and IF1-R30, α-GSDLDAST does not establish specific interactions with IF1. Since k_{off} grossly increases with the number of glycine substitution mutations, this effect is likely due to steric hindrance decrease. The αDP-GSDLDAST motif forms pliers with βDP subunit, and its lateral chains probably contribute to limit IF1 movements within these pliers. It should be noted that αDP-GSDLDAST is not only close to IF1, but also to the ^{115}KMQLL^{119} motif of the γ subunit. Therefore contacts between α-GSDLDAST and the foot of γ subunit (^{115}KMQLL^{119}) may contribute to the rigidity of pliers. Although quite modest, the effect of γ-M116G-Q117G mutation is detectable, and is therefore consistent with this view. A more extensive mutagenesis of this region of γ would be susceptible to confirm or infirm this proposal.

Among the α subunit residues we have mutated, one or several of the five residues bordering IF1 midpart (αE357, αY399, αR400, αV402, αQ418) slightly contribute to the inhibited complex stability. Their simultaneous mutation into their non-mitochondrial counterparts results in a 2.5-fold k_{off} increase. Except for V402L, these mutations globally decrease the volume of the lateral chains. Thus some of these residues probably limit movements when IF1 is trapped in the cavity between αDP and βDP. Compared to α-GSDLDAST, the effect of mutagenesis is much less important. This could be due to the nature of the mutations, to the relative remoteness of mutated residues from IF1 suggested by the yeast crystal, or to the lack of stabilizing interaction with the γ subunit.

Residues playing the major role in stabilization of the inhibited complex were found in regions of α and β subunits that interact not only with IF1, but also with the foot of γ subunit. This supports the idea that a part of the stabilization energy of the inhibited complex is brought by α–γ and/or β–γ interactions.

As for k_{on}, it is reasonable to wonder whether k_{off} changes might result from alterations of the enzyme catalytic properties. This is probably not the case, because contrary to k_{on}, k_{off} is practically insensitive to the catalytic state experienced by the enzyme before IF1 addition (Fig. 3c). This is consistent with the proposal that IF1 is released from the tightly bound inhibited complex without passing through the intermediate loose state (see Appendix A and Supplementary Material).

4.5. Possible distortion of F_1-ATPase by IF1 binding

Since IF1 locking may involve contacts not only between the inhibitory peptide and ATP synthase, but also between different subunits of the enzyme, it is interesting to know how the latter can be distorted by IF1 binding. This can be done by comparing the published structures of F_1-ATPase with and without bound IF1. In most of IF1-free bovine crystals (*e.g.* pdb files *1bmf*, *1e79* and *2jdi* for *F_1-ATPase*, *2xnd* for *c_8-F_1-ATPase*) F_1-ATPases have similar conformations [12,52,53,3]. This is not the case for yeast. The crystal of IF1-free yeast F_1-ATPase with two catalytic nucleotides bound (pdb file *2hld*) contains three non-equivalent copies of the complex [54]. Two copies (I and II) have the major part of their structure solved. Copy II looks similar to bovine F_1-ATPase, but copy I is different. In particular the (αβ)DP catalytic interface of copy I is noticeably more open, as in crystallized yeast c_{10}-F_1-ATPase (pdb file *3zry*) [4]. In the following, copy II of pdb file *2hld* will be considered the most probable conformation of IF1-free yeast F_1-ATPase.

The crystallographic structures of F_1-ATPase with bound IF1 are *2v7q* for bovine [10] and *3zia* for yeast [11]. The latter contains two quite similar copies. In bovine, comparison of these structures with IF1-free structures as defined above suggests that interaction between the motifs homologous to αDP-^{409}GSDLDAST^{416} and γ^{116}MQLL^{119} occurs only after IF1 binding. This IF1-dependent distortion due to incomplete closure of (αβ)DP catalytic interface is not observed in yeast crystals, where the two motifs always appear in contact. The situation is different for the contact between βDP-DELSEQD motif (especially E395) and γ subunit. In yeast this interaction seems to be a consequence of IF1 binding. In bovine and in yeast the γ subunit residues interacting with βDP-E395 are not homologous, and in bovine their interaction does not seem to depend on IF1 binding.

Comparison of structures with and without IF1 also provides a clue for the role of αS410 in ^{409}GSDLDAST^{416} motif. The k_{off} decrease due to αS410G mutation suggests that αS410 decreases the stability of the IF1-inhibited complex. This residue makes a H-bond with αA406 in the yeast IF1-free crystal, but not in the yeast IF1-inhibited one. This H-bond could stabilize the loop containing S410 in its non-inhibited conformation, and therefore its suppression by mutagenesis might displace the equilibrium towards the conformation inhibited by IF1.

Examination of published structural data may help to know whether distortions of the catalytic interface by IF1 binding indirectly contribute to the stabilization of the inhibited complex, by favouring contacts between the stator and the rotor. However, these distortions may differ between species. In yeast, the evidence for such distortions depends on the choice of the copy of IF1-free complex in the crystal.

4.6. Energetic considerations

K_d variations induced by the different mutations reflect IF1 binding energy variations. The relationship between the binding energy (in kJ mol^{-1}) and the equilibrium constant of dissociation (in M) is $\Delta G_0 = -5.7 \log_{10} K_d$ (at 25 °C). The variations observed in this work ranged between 2 kJ mol^{-1} (about doubling the K_d value) and 10 kJ mol^{-1} (multiplying K_d by about 70) when a single subunit was mutated. These values are moderate and range in the same order of magnitude as those previously obtained after deleting the IF1 N-terminal extremity [25]. This illustrates the fact that binding energy is shared between lots of interactions. We think that the lowest energetic contributions (2 kJ mol^{-1}) are not due to specific interactions, but to steric hindrance limiting the mobility of IF1 within its binding site. Although low, these values are significant and may reveal proximities that cannot be deduced from structural data. For example, the couple βDP-E471-A474 is in contact with IF1 residues that are not visible in the yeast IF1-inhibited F_1-ATPase complex.

Interestingly, the loss of binding energy due to the combination of ^{11}DLD^{13} deletion in α and E395G in β is 16.6 kJ mol^{-1}. It is the sum of energy losses associated with separate mutations: 10.5 kJ mol^{-1} for α-^{11}DLD^{13} deletion and 6.0 kJ mol^{-1} for β-E395G. These numbers should be cautiously considered regarding uncertainties on the K_d value for the WT enzyme. Nevertheless, they suggest that α-GSDLDAST and β-DELSEQD motifs would independently contribute to IF1 binding energy. This example shows that combinations of different mutations could reveal possible cooperativity between different contact zones within the IF1-inhibited F_1-ATPase complex.

4.7. An outline of IF1 binding process

Our work together with structural data analysis and previous functional studies allow proposing the following sequence of events for inhibition of mitochondrial ATP synthase by IF1. First, IF1 midpart is recognized by one of the three catalytic αβ interfaces. It mainly interacts with the very C-terminal extremity of β subunit, but also somehow with the GSDLDAST motif of α subunit. After loose IF1 binding, the enzyme still experiences a fraction of turn and the catalytic interface that has just bound IF1 closes and becomes (αβ)DP, which results in IF1 trapping. Thus αDP-GSDLDAST and βDP-DELSEQD motifs become elements of pliers, which encage IF1 with the α-motif interacting more tightly with IF1. The role of β subunit C-terminal extremity becomes much less important than during the initial step. In addition, other αDP residues flanking IF1 midpart modestly contribute to trapping,

probably by limiting IF1 movements within the crevice between αDP and βDP. The rigidity of the pliers formed by αDP-GSDLDAST and βDP-DELSEQD is partially ensured by their interactions with the foot of the γ subunit. These α–γ and β–γ interactions could be slightly different in bovine and yeast enzymes according to the structure comparisons, which suggest that IF1 binding brings αDP-GSDLDAST closer to γ in bovine and brings βDP-DELSEQD closer to γ in yeast. Another contribution to locking comes from the N-terminal part of IF1 which penetrates into the complex and interacts with γ and internal parts of α and β subunits. IF1–F17, located at the boundary between the α-helical midpart of IF1 and the flexible N-terminal extremity, also plays a key role in stabilization of the inhibited complex [46,25]. To make exhaustive this dynamic scheme, a more systematic mutagenesis programme should be undertaken. More than the precise role of key residues, the present work reveals the global role of different motifs and regions in the different steps of inhibition by IF1. This approach significantly improves our knowledge of its mechanism. Other aspects remain to be elucidated, like the possible energetic interferences between the different locking events and their time-sequence. This will be a challenge for future studies.

Acknowledgements

Thanks are due to Dr Marie-France Giraud for her help in microbiology of *S. cerevisiae* W303-1A-*Δatp1Δatp2*. We are indebted to Gwénaëlle Moal for her excellent technical help. We particularly thank Amina Boudghene Stambouli for technical assistance in the mutagenesis of γ subunit.

Appendix A

Model of two-step IF1 binding to the catalytic sector of ATP synthase. The kinetic scheme of IF1 binding is presented below (Scheme A1). Briefly, IF1 loosely binds with different rates to the enzyme having two or three filled catalytic sites.[3] It is locked within the enzyme only when three catalytic sites are filled. The resulting inhibited complex may directly release IF1, with a low rate, without passing through the loosely bound states. This is the minimum model that accounts for past and present experimental data. Reasonings leading to this model are developed in the Supplementary Material.

$$\begin{array}{ccc} ES_2 + I & \underset{k_{off}}{\overset{k^{A}_{on}}{\rightleftharpoons}} & I.ES_2 \\ +S\downarrow\uparrow(K_m) & & +S\downarrow\uparrow(K_m) \\ ES_3 + I & \underset{k_{off}}{\overset{k^{B}_{on}}{\rightleftharpoons}} & I.ES_3 \xrightarrow{k_{lock}} I.E' \xrightarrow{k'_{off}} (ES_2 \underset{K_m}{\overset{+S}{\rightleftharpoons}} ES_3) \end{array}$$

Scheme A1. Kinetic model for IF1 binding.

Meaning of the different states and associated rate constants. ES_2 and ES_3 are active forms of the enzyme with two or three catalytic sites occupied by ATP and/or ADP during steady state ATP hydrolysis, S is the substrate. K_m is the Michaelis constant for ATP hydrolysis because the catalytic turnover rate is proportional to the fraction of enzymes containing three nucleotides. ES_2 and ES_3 bind IF1 with the association rate constants k^{A}_{on} and k^{B}_{on}, to form $I.ES_2$ and $I.ES_3$ states which contain loosely bound IF1. The dissociation rate constant of loosely bound IF1 (k_{off}) is assumed to be the same for $I.ES_2$ and $I.ES_3$. The locking step (k_{lock} constant) converts $I.ES_3$ state (loosely bound IF1) into I.E′ state (tightly bound IF1) which is inactive. During this conversion one ADP molecule is probably released. I.E′ releases IF1 with a dissociation rate constant k'_{off}.

Description of the two-step binding of IF1. The active states, ES_2 and ES_3 states are transformed into $I.ES_2$ and $I.ES_3$ by loose IF1 binding. As explained in the Supplementary Material, the steady state concentration of these intermediate is very low, because loosely bound IF1 is either released (k_{off}), or trapped (k_{lock}) at a high rate. IF1 trapping is induced by catalytic turnover. Only $I.ES_3$ is able to lock IF1, because $I.ES_2$ activity is very low, like ES_2 activity. Since catalytic activity of $I.ES_3$ immediately results in IF1 trapping, only a fraction of turn can be performed between loose and tight IF1 binding. IF1 binding and release (seconds range) are much slower than the binding and release of substrate and products (milliseconds range). For this reason ES_3/ES_2 and $I.ES_3/I.ES_2$ ratios remain constant during all the decay of activity.

Measured ATPase activity. Only the states without IF1 contribute to the measured activity, because states with loosely bound IF1 are always at negligible concentration. Notably, $I.ES_3$ disappears during the first rotor turn following loose IF1 binding. Therefore the decay of ATPase activity strictly follows the disappearance of IF1-free states.

Relationship between mechanistic and measured parameters. As explained in the Supplementary Material, this model is consistent with a first-order inhibition reaction if IF1 concentration is constant. The time-dependent decay of activity is mono-exponential, and the inhibition rate constant k_{app} is:

$$k_{app} = k^{*}_{on}[I] + k'_{off}. \tag{A1}$$

This equation is the same as Eq. (2) (Materials and methods), but with the following features:

The asterisk indicates here that the association rate constant k^{*}_{on} is actually a function of several kinetic constants and a function of MgATP concentration.

k'_{off} is not identified with the dissociation constant of loosely bound states, but with the dissociation rate constants of I.E′ in Scheme (A1).

The value of k^{*}_{on} is:

$$k^{*}_{on} = \frac{\dfrac{k^{A}_{on}}{1 + [MgATP]/K_m} + \dfrac{k^{B}_{on}}{1 + K_m/[MgATP]}}{1 + \dfrac{k_{off}}{k_{lock}}(1 + K_m/[MgATP])}. \tag{A2}$$

This function contains three parameters than can be experimentally determined: k^{A}_{on}, k^{B}_{on}, and the ratio k_{off}/k_{lock}. An example of such a determination is given in the Results Section (see Fig. 3).

At high MgATP concentration, which is the most common experimental condition in this work, one obtains:

$$\lim_{[MgATP]\to\infty} k^{*}_{on} = k^{B}_{on}. \tag{A3}$$

This means that at high MgATP concentration, the measured IF1 binding rate constant is the true constant of IF1 binding to the enzyme saturated with MgATP.

Appendix B. Supplementary data

Supplementary data to this article can be found online at http://dx.doi.org/10.1016/j.bbabio.2014.01.023.

[3] In the present model we have assumed that the maximum rate of ATP hydrolysis was reached when the three catalytic sites were filled (the so-called "tri-site" catalytic mechanism [55,56]). This view is questioned by authors who support a mechanism in which the maximum rate is reached with only two filled catalytic sites ("bi-site" mechanism [57]). If the second proposal is correct, ES_2 and ES_3 must be replaced respectively by ES_1 and ES_2, the K_m will therefore correspond to the half-saturation of the second catalytic site, and our model of MgATP-dependent IF1 binding will remain valid.

References

[1] P. Mitchell, Coupling of phosphorylation to electron and hydrogen transfer by a chemi-osmotic type of mechanism, Nature 191 (1961) 144–148.
[2] H. Noji, R. Yasuda, M. Yoshida, K. Kinosita, Direct observation of the rotation of F-$_1$-ATPase, Nature 386 (1997) 299–302.
[3] I.N. Watt, M.G. Montgomery, M.J. Runswick, A.G.W. Leslie, J.E. Walker, Bioenergetic cost of making an adenosine triphosphate molecule in animal mitochondria, Proc. Natl. Acad. Sci. U. S. A. 107 (2010) 16755–16756.
[4] A. Dautant, J. Velours, M.-F. Giraud, Crystal structure of the Mg.ADP-inhibited state of the yeast F_1c_{10}-ATP synthase, J. Biol. Chem. 285 (2010) 29502–29510.
[5] P.D. Boyer, The ATP synthase — a splendid molecular machine, Annu. Rev. Biochem. 66 (1997) 717–749.
[6] H. Itoh, A. Takahashi, K. Adachi, H. Noji, R. Yasuda, M. Yoshida, K. Kinosita, Mechanically driven ATP synthesis by F_1-ATPase, Nature 427 (2004) 465–468.
[7] M.E. Pullmann, G.C. Monroy, A naturally occurring inhibitor of mitochondrial adenosine triphosphatase, J. Biol. Chem. 238 (1963) 3762–3768.
[8] H. Matsubara, T. Hase, T. Hashimoto, K. Tagawa, Amino acid sequence of an intrinsic inhibitor of mitochondrial ATPase from yeast, J. Biochem. 90 (1981) 1159–1165.
[9] E. Cabezón, M.J. Runswick, A.G. Leslie, J.E. Walker, The structure of bovine IF(1), the regulatory subunit of mitochondrial F-ATPase, EMBO J. 20 (2001) 6990–6996.
[10] J.R. Gledhill, M.G. Montgomery, A.G.W. Leslie, J.E. Walker, How the regulatory protein, IF1, inhibits F_1-ATPase from bovine mitochondria, Proc. Natl. Acad. Sci. U. S. A. 104 (2007) 15671–15676.
[11] G.C. Robinson, J.V. Bason, M.G. Montgomery, I.M. Fearnley, D.M. Mueller, A.G.W. Leslie, J.E. Walker, The structure of F_1-ATPase from *Saccharomyces cerevisiae* inhibited by its regulatory protein IF1, Open Biol. 3 (2013) 120164.
[12] J.P. Abrahams, A.G.W. Leslie, R. Lutter, J.E. Walker, Structure at 2.8 Å resolution of F-$_1$-ATPase from bovine heart mitochondria, Nature 370 (1994) 621–628.
[13] V. Kabaleeswaran, H. Shen, J. Symersky, J.E. Walker, A.G.W. Leslie, D.M. Mueller, Asymmetric structure of the yeast F_1-ATPase in the absence of bound nucleotides, J. Biol. Chem. 284 (2009) 10546–10551.
[14] K. Schwerzmann, P.L. Pedersen, Regulation of the mitochondrial ATP synthase/ATPase complex, Arch. Biochem. Biophys. 250 (1986) 1–18.
[15] R.J. Van de Stadt, B.L. de Boer, K. Van Dam, The interaction between the mitochondrial ATPase (F_1) and the ATPase inhibitor, Biochim. Biophys. Acta 292 (1973) 338–349.
[16] I. Husain, D.A. Harris, ATP synthesis and hydrolysis in submitochondrial particles subjected to an acid–base transition. Effects of the ATPase inhibitor protein, FEBS Lett. 160 (1983) 110–114.
[17] J. Power, R.L. Cross, D.A. Harris, Interaction of F_1-ATPase from ox heart mitochondria with its naturally occurring inhibitor protein. Studies using radio-iodinated inhibitor protein, Biochim. Biophys. Acta 724 (1983) 128–141.
[18] G. Klein, P.V. Vignais, Effect of the protonmotive force on ATP-linked processes and mobilization of the bound natural ATPase inhibitor in beef heart submitochondrial particles, J. Bioenerg. Biomembr. 15 (1983) 347–362.
[19] I. Husain, P.J. Jackson, D.A. Harris, Interaction between F_1-ATPase and its naturally occurring inhibitor protein. Studies using a specific anti-inhibitor antibody, Biochim. Biophys. Acta 806 (1985) 64–74.
[20] G. Lippe, M.C. Sorgato, D.A. Harris, Kinetics of the release of the mitochondrial inhibitor protein. Correlation with synthesis and hydrolysis of ATP, Biochim. Biophys. Acta 933 (1988) 1–11.
[21] G. Lippe, M.C. Sorgato, D.A. Harris, The binding and release of the inhibitor protein are governed independently by ATP and membrane potential in ox-heart submitochondrial vesicles, Biochim. Biophys. Acta 933 (1988) 12–21.
[22] G. Klein, M. Satre, P. Vignais, Natural protein ATPase inhibitor from *Candida utilis*. Binding properties of the radiolabeled inhibitor, FEBS Lett. 84 (1977) 129–134.
[23] V. Corvest, C. Sigalat, R. Venard, P. Falson, D.M. Mueller, F. Haraux, The binding mechanism of the yeast F_1-ATPase inhibitory peptide: role of catalytic intermediates and enzyme turnover, J. Biol. Chem. 280 (2005) 9927–9936.
[24] V. Corvest, C. Sigalat, F. Haraux, Insight into the bind-lock mechanism of the yeast mitochondrial ATP synthase inhibitory peptide, Biochemistry 46 (2007) 8680–8688.
[25] T. Andrianaivomananjaona, M. Moune-Dimala, S. Herga, V. David, F. Haraux, How the N-terminal extremity of *Saccharomyces cerevisiae* IF1 interacts with ATP synthase: a kinetic approach, Biochim. Biophys. Acta 1807 (2011) 197–204.
[26] J.V. Bason, M.J. Runswick, I.M. Fearnley, J.E. Walker, Binding of the inhibitor protein IF1 to bovine F_1-ATPase, J. Mol. Biol. 406 (2011) 445–453.
[27] M. Minet, M.E. Dufour, F. Lacroute, Complementation of *Saccharomyces cerevisiae* auxotrophic mutants by *Arabidopsis thaliana* cDNAs, Plant J. 2 (1992) 417–422.
[28] A. Wach, A. Brachat, R. Poehlmann, P. Philippsen, New heterologous modules for classical or PCR-based gene disruptions in *Saccharomyces cerevisiae*, Yeast 10 (1994) 1793–1808.
[29] R. Venard, D. Brèthes, M.-F. Giraud, J. Vaillier, J. Velours, F. Haraux, Investigation of the role and mechanism of IF1 and STF1 proteins, twin inhibitory peptides which interact with the yeast mitochondrial ATP synthase, Biochemistry 42 (2003) 7626–7636.
[30] U.K. Laemmli, Cleavage of structural proteins during the assembly of the head of bacteriophage T4, Nature 227 (1970) 680–685.
[31] H. Schagger, G. von Jagow, Tricine-sodium dodecyl sulfate-polyacrylamide gel electrophoresis for the separation of proteins in the range from 1 to 100 kDa, Anal. Biochem. 166 (1987) 368–379.
[32] G. Arselin, J. Vaillier, P.V. Graves, J. Velours, ATP synthase of yeast mitochondria. Isolation of the subunit h and disruption of the ATP14 gene, J. Biol. Chem. 271 (1996) 20284–20290.
[33] F. Godard, E. Tetaud, S. Duvezin-Caubet, J.-P. di Rago, A genetic screen targeted on the F_0 component of mitochondrial ATP synthase in *Saccharomyces cerevisiae*, J. Biol. Chem. 286 (2011) 18181–18189.
[34] M. Rak, E. Tetaud, F. Godard, I. Sagot, B. Salin, S. Duvezin-Caubet, P.P. Slonimski, J. Rytka, J.-P. di Rago, Yeast cells lacking the mitochondrial gene encoding the ATP synthase subunit 6 exhibit a selective loss of complex IV and unusual mitochondrial morphology, J. Biol. Chem. 282 (2007) 10853–10864.
[35] L. Lefebvre-Legendre, B. Salin, J. Schaeffer, D. Brèthes, A. Dautant, S.H. Ackerman, J.-P. di Rago, Failure to assemble the alpha 3 beta 3 subcomplex of the ATP synthase leads to accumulation of the alpha and beta subunits within inclusion bodies and the loss of mitochondrial cristae in *Saccharomyces cerevisiae*, J. Biol. Chem. 280 (2005) 18386–18392.
[36] Y.M. Milgrom, An ATP dependence of mitochondrial F_1-ATPase inactivation by the natural inhibitor protein agrees with the alternating-site binding-change mechanism, FEBS Lett. 246 (1989) 202–206.
[37] E. Cabezón, P.J. Butler, M.J. Runswick, R.J. Carbajo, J.E. Walker, Homologous and heterologous inhibitory effects of ATPase inhibitor proteins on F-ATPases, J. Biol. Chem. 277 (2002) 41334–41341.
[38] T.M. Duncan, V.V. Bulygin, Y. Zhou, M.L. Hutcheon, R.L. Cross, Rotation of subunits during catalysis by *Escherichia coli* F_1-ATPase, Proc. Natl. Acad. Sci. U. S. A. 92 (1995) 10964–10968.
[39] K.Y. Hara, H. Noji, D. Bald, R. Yasuda, K. Kinosita, M. Yoshida, The role of the DELSEED motif of the β subunit in rotation of F_1-ATPase, J. Biol. Chem. 275 (2000) 14260–14263.
[40] N. Mnatsakanyan, A.M. Krishnakumar, T. Suzuki, J. Weber, The role of the DELSEED-loop of ATP synthase, J. Biol. Chem. 284 (2009) 11336–11345.
[41] M. Tanigawara, K.V. Tabata, Y. Ito, J. Ito, R. Watanabe, H. Ueno, M. Ikeguchi, H. Noji, Role of the DELSEED loop in torque transmission of F_1-ATPase, Biophys. J. 103 (2012) 970–978.
[42] K.Y. Hara, Y. Kato-Yamada, Y. Kikuchi, T. Hisabori, M. Yoshida, The role of the βDELSEED motif of F_1-ATPase; propagation of the inhibitory effect of the ε subunit, J. Biol. Chem. 276 (2001) 23969–23973.
[43] J.S. Stout, B.E. Partridge, D.A. Dibbern, S.M. Schuster, Peptide analogs of the beef heart mitochondrial F_1-ATPase inhibitor protein, Biochemistry 32 (1993) 7496–7502.
[44] M.J. van Raaij, G.L. Orriss, M.G. Montgomery, M.J. Runswick, I.M. Fearnley, J.M. Skehel, J.E. Walker, The ATPase inhibitor protein from bovine heart mitochondria: the minimal inhibitory sequence, Biochemistry 35 (1996) 15618–15625.
[45] M.S. Lebowitz, P.L. Pedersen, Protein inhibitor of mitochondrial ATP synthase: relationship of inhibitor structure to pH-dependent regulation, Arch. Biochem. Biophys. 330 (1996) 342–345.
[46] N. Ichikawa, A. Karaki, M. Kawabata, S. Ushida, M. Mizushima, T. Hashimoto, The region from phenylalanine-17 to phenylalanine-28 of a yeast mitochondrial ATPase inhibitor is essential for its ATPase inhibitory activity, J. Biochem. 130 (2001) 687–693.
[47] R.S. Lee, J. Pagan, M. Satre, P.V. Vignais, A.E. Senior, Identification of a mutation in *Escherichia coli* F_1-ATPase beta-subunit conferring resistance to aurovertin, FEBS Lett. 253 (1989) 269–272.
[48] M.J. van Raaij, J.P. Abrahams, A.G.W. Leslie, J.E. Walker, The structure of bovine F-$_1$-ATPase complexed with the antibiotic inhibitor aurovertin B, Proc. Natl. Acad. Sci. U. S. A. 93 (1996) 6913–6917.
[49] J. Santolini, C. Minoletti, J.M. Gomis, C. Sigalat, F. André, F. Haraux, An insight into the mechanism of inhibition and reactivation of the F_1-ATPases by tentoxin, Biochemistry 41 (2002) 6008–6018.
[50] A. Avni, J.D. Anderson, N. Holland, J.D. Rochaix, Z. Gromet-Elhanan, M. Edelman, Tentoxin sensitivity of chloroplasts determined by codon 83 of beta subunit of proton-ATPase, Science 257 (1992) 1245–1247.
[51] W.C. Tucker, Z. Du, R. Hein, Z. Gromet-Elhanan, M.L. Richter, Role of the ATP synthase alpha-subunit in conferring sensitivity to tentoxin, Biochemistry 40 (2001) 7542–7548.
[52] C. Gibbons, M.G. Montgomery, A.G.W. Leslie, J.E. Walker, The structure of the central stalk in bovine F_1-ATPase at 2.4 Å resolution, Nat. Struct. Biol. 7 (2000) 1055–1061.
[53] M.W. Bowler, M.G. Montgomery, A.G.W. Leslie, J.E. Walker, Ground state structure of F_1-ATPase from bovine heart mitochondria at 1.9 Å resolution, J. Biol. Chem. 282 (2007) 14238–14242.
[54] V. Kabaleeswaran, N. Puri, J.E. Walker, A.G.W. Leslie, D.M. Mueller, Novel features of the rotary catalytic mechanism revealed in the structure of yeast F_1 ATPase, EMBO J. 25 (2006) 5433–5442.
[55] J. Weber, S. Wilke-Mounts, R.S. Lee, E. Grell, A.E. Senior, Specific placement of tryptophan in the catalytic sites of *Escherichia coli* F_1-ATPase provides a direct probe of nucleotide binding: maximal ATP hydrolysis occurs with three sites occupied, J. Biol. Chem. 268 (1993) 20126–20133.
[56] H. Ren, S. Bandyopadhyay, W.S. Allison, The $\alpha_3(\beta Met^{222}Ser/Tyr^{345}Trp)^3\gamma$ subcomplex of the TF_1-ATPase does not hydrolyze ATP at a significant rate until the substrate binds to the catalytic site of the lowest affinity, Biochemistry 45 (2006) 6222–6230.
[57] Y.M. Milgrom, R.L. Cross, Rapid hydrolysis of ATP by mitochondrial F_1-ATPase correlates with the filling of the second of three catalytic sites, Proc. Natl. Acad. Sci. U. S. A. 102 (2005) 13831–13836.